Chapter 4: **CRYSTALLOGRAPHIC CHARACTERISATION**

An important aspect of the characterisation of these crystals is to determine their structure by focusing on the positions of the different dopants. Also, to fully characterise the crystals for latter use as laser emitters, we analysed how their structure was affected by temperature. All these aspects are described in this Chapter.

4.1. The structure of $RbTiOPO_4$.

At room temperature, the crystal symmetry of RTP is orthorhombic and belongs to the non-centrosymmetric space group *Pna2₁* with the lattice parameters ***a*** = 12.974(2) Å, ***b*** = 6.494(3) Å and ***c*** = 10.564(6) Å.[188] The primitive cell contains eight formula units and four asymmetric units, each made up of two formula units.

The structure of this family of compounds may be described as a network of chains of very distorted TiO_6 octahedra, in which the Ti^{4+} ions are displaced from the centres of the octahedra, and slightly distorted PO_4 tetrahedra, which are coupled at their vertices. The TiO_6 octahedra are linked by PO_4 octahedra with periodic bond chains of -PO_4-TiO_6- in the ***a*** direction and along the ***a-c*** diagonal (see Figure 4.1). Ti(1) and Ti(2) octahedra alternate along the ***c*** direction to form helicoidal chains of linked TiO_6 octahedra. The distortion of the TiO_6 octahedra results in four medium-length Ti-O bonds, one long Ti-O bond and one short Ti-O bond. The long and short bonds, which link the TiO_6 rows, involve two O^{2-} ions. These ions, which are independent because they do not belong to the PO_4 groups, are denoted by OT(1) and OT(2). Luminescence studies have shown that the bonds in the titanate chain in the KTP structural family are quite covalent. Also, there is some de-localisation of the electronic charge along the directions of the chain.[189] If we take the plane containing the central Ti atom and the two OT oxygen atoms as the equatorial plane of the Ti octahedra, we find that in the case of $Ti(1)O_6$ this plane is almost parallel to the (010) plane (see Table 6 in *paper VII*), the ***c*** axis is almost parallel to the $OT(1)^{iii}$-$OT(2)^{ii}$ vector and the ***a*** axis is approximately parallel to the $OT(1)^{iii}$-O(1) vector. The $O(5)^{ii}$ and $O(6)^{iii}$ atoms are out of the plane and bonded to Ti(1) along a line that is almost parallel to the ***b*** axis (see Figure 4.1). In the $Ti(2)O_6$ octahedron, the equatorial plane is almost parallel to the (100) plane and made up of $O(7)^{iii}$, O(8), $OT(1)^{iii}$ and OT(2) atoms. The ***c*** axis is approximately parallel to the O(8)-$OT(1)^{iii}$ vector and the apical O(3) and $O(4)^{iv}$ atoms are bonded to Ti(2) along a line almost parallel to the ***a*** axis (see Figure 4.1).

As we have seen, the TiO_6 octahedra and the PO_4 tetrahedra form a three-dimensional network that has large holes with two different crystallographic sites for the same cation. The cavities are slightly stretched in the ***c*** direction. The positions of the alkali metal ions are in both halves of the cavities that form open channels along the ***c*** axis, which in the case of KTP results in high ionic conductivity. The two Rb^+ cations occupy positions related by the 2_1 screw axis (see Figure 4.1(c)). Rb gives nine-coordination in both sites.

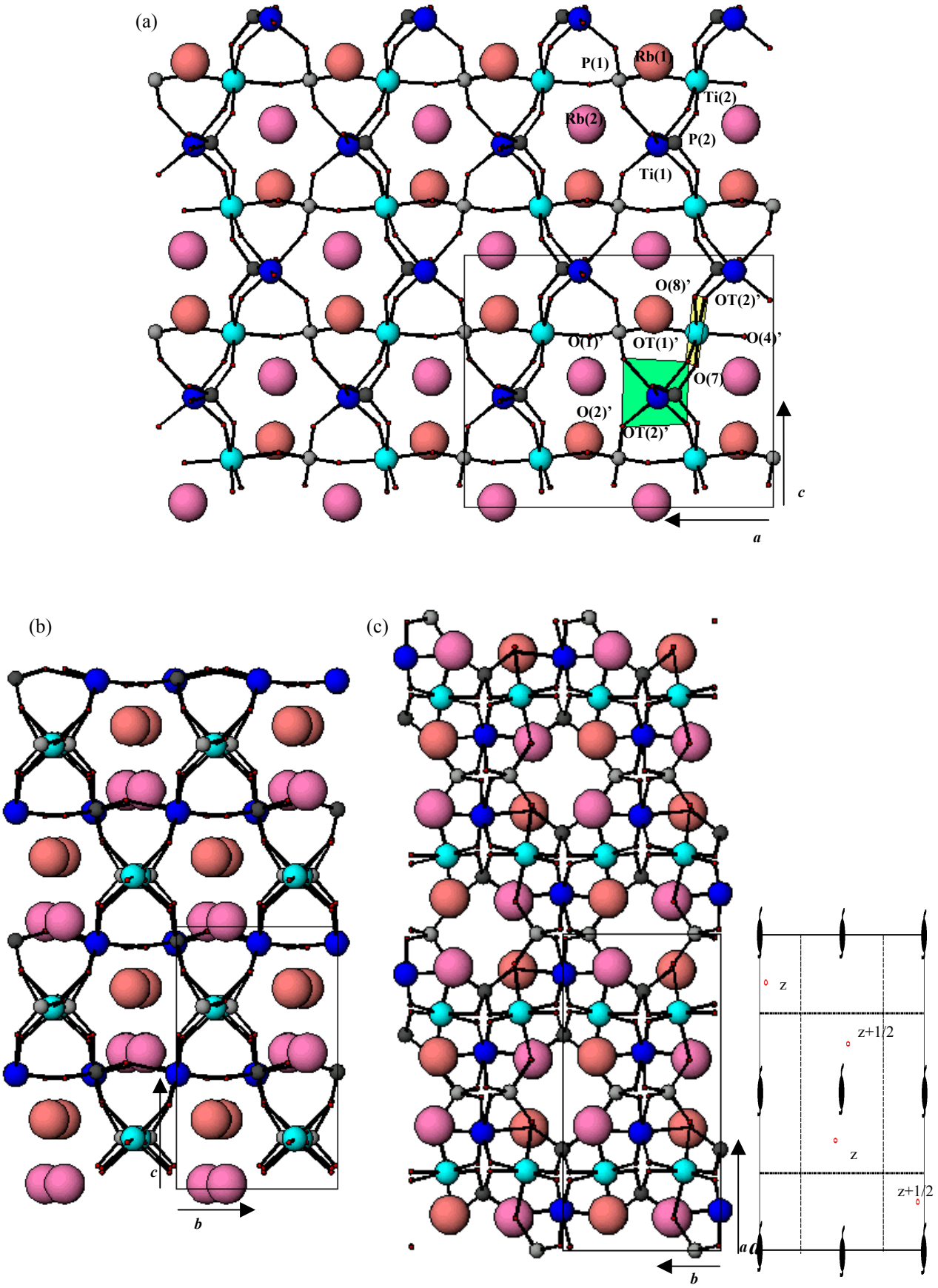

Figure 4.1. *View of the structure of the RTP family of crystals illustrating the connected paths formed by alternating $Ti(1)O_6$ and $Ti(2)O_6$ octahedra. Projections parallel to the (a) [010], (b) [100] and (c) [001] directions.*

4.1.1. Effect of temperature on $RbTiOPO_4$ structure.

Crystals leading to an electric polarisation when the temperature changes, or vice versa, are called pyroelectric crystals. Many pyroelectric crystals exhibit a spontaneous polarisation which can be reversed by applying an external electric field; these are called ferroelectric crystals. Yanovskii and Voronkova[190] first reported that RTP crystals are ferroelectric at room temperature, with the ***c*** axis as the polar axis. However, the system is not ferroelectric in the conventional sense because a strong coercive force and a high ionic conductivity seem to make it impossible to reverse the polarisation. However, when the polarisation can be reversed, this is due to relatively small shifts within the crystal structure that turn the crystal into its polar twin. Spontaneous polarisation is normally reversed in different parts of the crystal known as ferroelectric domains. The KTP isostructurals are uniaxial ferroelectrics, with spontaneous polarisation along the ***c*** axis, and the domains are formed with walls perpendicular to the ***a*** axis, because, energetically, this is the most favourable configuration.[191] Ferroelectric crystals have a transition temperature, the Curie point (T_c), above which the structure becomes paraelectric and non-polar; the structure of the crystal structure then becomes more symmetrical.[192]

When RTP is heated to 1090-1198 K, the orthorhombic non-centrosymmetric phase becomes an orthorhombic paraelectric structure of symmetry *Pnan*. The structural phase transition is assumed to be displacive and may be described as a continuous second order transition, of both displacive and order-disorder types.[193,194] The high-temperature paraelectric *Pnan* centrosymmetric structure of this family of crystals was determined by single-crystal neutron diffraction for $TlTiOPO_4$.[195]

No complete study of phase transitions in RTP with temperature has yet been published and the results in the literature for the different phase transitions of this material are inconsistent. In Figure 3(a) in *paper VIII*, which for RTP shows the evolution of the powder diffraction pattern with temperature, we can see that the RTP phase extended from room temperature to 1323 K as the temperature increased. Over 1323 K, the high-temperature cubic phase of RTP, namely $RbTiPO_5$, and the decomposition of this cubic phase were observed. A thermal hysteresis of a minimum value of 50 K was detected in the phase transition from the orthorhombic phase to the cubic phase in RTP. $RbTiPO_5$ was detected in all temperature ranges of the cooling cycle, but this was a minor phase.

These results show that the phase transition of RTP from the ferroelectric ($Pna2_1$) phase to the paraelectric (*Pnan*) phase could not be detected by analysing the X-ray powder diffraction files of the phases because all the peaks that produced extinction with the change of symmetry from $Pna2_1$ to *Pnan* had so little intensity that the existence or extinction of these peaks could not be confirmed. To observe this phase transition we studied how the ***c*** parameter evolved with temperature (see Figure 2 in *paper VIII*). This way of visualising the phase transition from the ferroelectric phase to the paraelectric phase

as the ***c*** parameter evolves with temperature is not reported in the literature for this family of compounds.

Tables 2 and 3 in *paper VIII* summarise the different phase transitions of RTP crystals with temperature. From these results we propose the following chemical reaction for RTP with temperature:

$$RbTiOPO_4 \text{ (ferroelectric, } Pna2_1) \overset{T_c}{\leftrightarrow} RbTiOPO_4 \text{ (paraelectric, } Pnan) \overset{T_{o\rightarrow c}}{\leftrightarrow} RbTiPO_5 \text{ (cubic, } Fd\bar{3}m) \overset{T_d}{\rightarrow} Rb_2O\ (g) + P_2O_5\ (g) + TiO_2 \text{ (rutile)},$$

where T_c is the Curie temperature, $T_{o\rightarrow c}$ is the phase transition temperature for the orthorhombic RTP phase to the cubic $RbTiPO_5$ phase and T_d is the temperature of decomposition.

4.2. The location of Nb in the structure of $RbTiOPO_4$:Nb crystals.

We solved the structure of $Rb_{0.855}Ti_{0.955}Nb_{0.045}OPO_4$ by single crystal X-ray diffraction. The unit cell parameters were ***a*** = 12.947(3) Å, ***b*** = 6.498(3) Å and ***c*** = 10.579(7) Å and Z = 8. Parameter ***a*** was shorter, ***b*** was slightly longer and ***c*** was clearly longer than in the RTP structure. Crystal data, refinement and atomic coordinates are given in Tables 1 and 2 in *paper VII*.

The main characteristic of this structure is that we obtained the enantiomorphic image of pure RTP. This feature was also observed in the KTP:Nb structure when we compared it to that of pure KTP.[119,196]

Table 3 in *paper VII* shows the occupation factors of the $Rb_{0.855}Ti_{0.955}Nb_{0.045}OPO_4$ structure. The occupancies of the crystallographically independent positions for rubidium cations were 0.832(5) for Rb(1) and 0.878(5) for Rb(2). This follows the same trend as in the KTP:Nb samples. The occupancies of Ti sites were 0.910(8) and 0.090(8) for Ti and Nb, respectively, in Ti(1) positions, and 1.000(8) and 0.000(8) for the same cations in the Ti(2) position. Nb clearly tends to occupy only the Ti(1) position.

Although EPMA measurements did not establish the stabilisation of Rb vacancies in this type of crystals, refining the structure gives a clearly loss of Rb in the crystals that contained Nb. This is an interesting aspect of doping RTP with Nb: the ability of the material to self-compensate electrically for pentavalent substitution through the loss of Rb atoms. The mean Rb-O bond length was greater in the $Rb_{0.855}Ti_{0.955}Nb_{0.045}OPO_4$ structure than in the structure of pure RTP. This is consistent with the expansion of the cages in the structure caused by the loss of Rb atoms. This was not observed in the $Rb(2)O_9$ cage, which had the same average Rb(2)-O bond length in the two materials: 2.993 Å (with Rb

vacant sites) and 2.992 Å (RTP). This indicates that when doping with pentavalent Nb^{5+} ions, Rb vacant sites are created mainly at the Rb(1) site.

Although Nb preferentially enters at the Ti(1) site, the Ti(1) and Ti(2) sites are very similar crystallographically. In the present concentration range, the distortion in the $Ti(2)O_6$ octahedra of RTP was not modified by doping with Nb, while the $Ti(1)O_6$ octahedra were more distorted than in the case of pure RTP (see Table 7 in *paper VII*). In our opinion, the preference for Nb^{5+} ions to occupy Ti(1) sites has an electrostatic origin rather than a steric one. If we compare the Ti-Rb bond distances in the $Rb_{0.855}Ti_{0.955}Nb_{0.045}OPO_4$ structure, we can see that these distances are rather shorter for the Ti(2) cation than for the Ti(1) cation (see Table 6 in *paper VII*). This implies that the electrostatic repulsion would be higher in the Ti(2) position than in the Ti(1) position. To avoid this electrostatic repulsion, therefore, Nb^{5+} tends to occupy Ti(1) positions.

4.2.1. Effects of Nb on the structure of $RbTiOPO_4$.

4.2.1.1. Variation of the lattice parameters of $RbTi_{1-x}Nb_xOPO_4$ with the concentration of Nb.

Figure 7 in *paper V* and Figure 1 in *paper VIII* plot the evolution of the lattice parameters and the volume of $RbTi_{1-x}Nb_xOPO_4$ crystals against the concentration of Nb^{5+} in the crystal. Parameters ***a*** and ***b*** decrease and parameter ***c*** increases as the concentration of Nb increases. Cell volume decreases as the concentration of Nb in the crystal increases. These changes in the lattice cells are different from those reported in the literature for KTP doped with Nb.[102]

The self-compensation of the crystals' excess electrical charge by the substitution of Ti^{4+} by Nb^{5+}, observed by a mechanism of creation of Rb^+ vacancies, may explain why substituting Ti^{4+} with an ion of a larger ionic radius did not, as was expected, enlarge the three cell parameters of the structure. The vacancies of Rb^+ may compensate both the crystal's excess electrical charge and the change in the cell parameters.

4.2.1.2. Thermal expansion coefficients.

Figure 2 in *paper VIII* shows how the lattice parameters and volume of the $RbTi_{1-x}Nb_xOPO_4$ (x = 0, 0.05 and 0.09) crystals evolve with temperature. The volume and parameters ***a*** and ***b*** increase as the temperature increases, but parameter ***c*** decreases. As with pure RTP, the change in the slope of the evolution of the ***c*** parameter marks the phase transition from the ferroelectric phase to the paraelectric phase. This change, which was also a function of the concentration of Nb, occurs at lower temperatures as the concentration of Nb in the crystal increases.

This material is interesting as a possible laser medium and may be subjected to temperatures above room temperature, caused by the conversion of an important part of the power pump in heat inside the laser material when it operates. We therefore need to know its linear thermal expansion coefficients to be able to predict how it behaves when the temperature increases. We calculated these coefficients from the slopes of the linear fittings of the relationship between ($\Delta L/L$), where L are the different cell parameters, and temperature in the different crystallographic directions. As expected by the symmetry of RTP, $\alpha_{i,j} = 0$ when $i \neq j$ and $\alpha_{i,j} \neq 0$ when $i = j$. The thermal expansion coefficients for $RbTi_{1-x}Nb_xOPO_4$ crystals with x = 0, 0.05 and 0.09 are given in Table 1 in *paper VIII*. The RTP:Nb thermal expansion coefficients, given for the first time, are slightly smaller than those for RTP. This implies that thermal anisotropy is lower, so the thermal stress the crystal is also lower.

4.2.1.3. Phase transition studies.

We used X-ray powder diffraction and DTA analyses to study the phase transitions of $RbTi_{0.91}Nb_{0.09}OPO_4$ crystals with temperature.

Figure 3(b) in *paper VIII* shows how the powder diffraction pattern of this crystal evolved as the temperature ranged from room temperature to 1373 K. The orthorhombic RTP was the only phase present between 973 K and 1173 K. Above 1173 K, the cubic $RbTiPO_5$ phase appeared, but unlike with pure RTP, this phase coexisted with the RTP orthorhombic phase between 1173 and 1323 K. Above 1323 K, the orthorhombic RTP phase disappeared and, as well as the cubic $RbTiPO_5$ phase, TiO_2 (rutile) and NbO_2 phases appeared. In the cooling cycle, $RbTiPO_5$, rutile and NbO_2 phases remained and the orthorhombic RTP phase did not appear. Unlike with pure RTP, the phase transition in this case was irreversible (see the DTA measurements in Figure 4 of *paper VIII*). A significant loss in weight coincided with the second peak of the thermogram, the one that corresponded to the decomposition of the cubic phase. Both the temperature of transition from the orthorhombic phase to the cubic phase and the decomposition of the cubic phase are functions of the content of Nb in the crystals. As the concentration of Nb in the crystals increased, the temperature of transition from the orthorhombic phase to the cubic phase decreased and the temperature of decomposition increased (see Figure 4 in *paper VIII*). This can be attributed to the stability of the cubic $RbTiPO_5$ phase induced by the presence of Nb. These results show that when Nb^{5+} substitutes the Ti^{4+}/Rb^{+} pair in RTP, the $RbTiPO_5$ cubic phase is stabilised by valence compensation.

Tables 2 and 3 in *paper VIII* summarise the phases observed with the changes $RbTi_{1-x}Nb_xOPO_4$ crystals with x = 0, 0.05 and 0.09. These results suggest that as the temperature increases the following chemical reaction takes place when Nb^{5+} is present in the crystals:

$RbTi_{1-x}Nb_xOPO_4$ (ferroelectric, $Pna2_1$) $\overset{T_c}{\leftrightarrow}$ $RbTi_{1-x}Nb_xOPO_4$ (paraelectric, $Pnan$) $\overset{T_{o\to c}}{\rightarrow}$ $RbTiPO_5$ (cubic, $Fd\bar{3}m$) + $RbTi_{1-x}Nb_xOPO_4$ $\overset{T_d}{\rightarrow}$ $RbTiPO_5$ (cubic, $Fd\bar{3}m$) + TiO_2 (rutile) + NbO_2

4.3. The location of Ln in the structure of $RbTiOPO_4$:(Nb,Ln) crystals.

We used the structure of $Rb_{0.855}Ti_{0.955}Nb_{0.045}OPO_4$ as the starting model for refining the structure of the $RbTi_{0.927}Nb_{0.056}Er_{0.017}OPO_4$ crystal from the results of neutron powder diffraction (NPD).

Table 1 in *paper III* and Table 5 in *paper VII* show the RT cell parameters, refined atomic coordinates and isotropic temperature factors of $RbTi_{0.927}Nb_{0.056}Er_{0.017}OPO_4$ structure from NPD. This table also shows the final reliability factors. Figure 4.2 illustrates the agreement between the observed NPD profiles and the calculated ones.

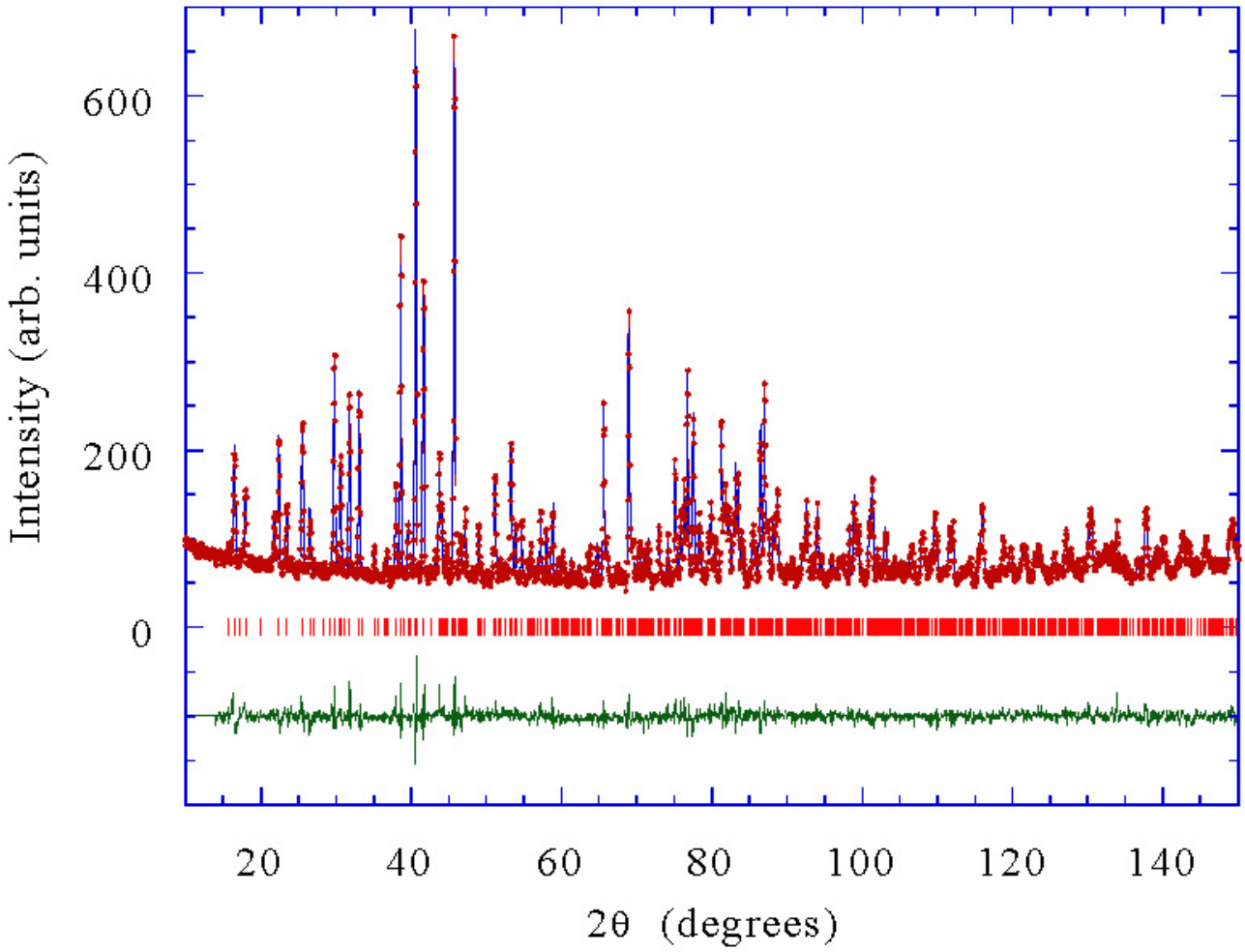

Figure 4.2. *Refined neutron diffraction pattern of* $RbTi_{0.927}Nb_{0.056}Er_{0.017}OPO_4$ *showing the observed (points), calculated (full line) and difference (bottom) Rietveld profiles at RT (D2B data).*

The volume of the unit cell was larger because of the increase in the atomic radius of Er^{3+}, but the distribution of this volume was not the same for all three cell parameters: ***a*** and ***b*** were 0.19 and 0.14 % longer, respectively, and ***c*** was 0.05 % shorter than the parameters of the $Rb_{0.855}Ti_{0.955}Nb_{0.045}OPO_4$ crystal. Our main aim in this study was to obtain reliable information about the distribution of the small concentration of Er and Nb cations in the structure. As expected, Nb and Er only went to Ti sites in the $RbTi_{0.927}Nb_{0.056}Er_{0.017}OPO_4$ structure. All the atomic positions, including oxygen and rubidium sites, were fully occupied. This was in contrast to the vacancies in rubidium sites in the RTP:Nb crystal.

When we fitted the occupation factors, the refinements always converged to the same scenario: Nb atoms only substituted Ti(1) atoms at the centre of the $Ti(1)O_6$ octahedra. The occupation factors converged to the values in Table 2 of *paper III* and Table 3 of *paper VII*. For Er, the refinements converged to the occupations 0.014(6) for Er(1) and 0.020(6) for Er(2). According to the errors, this is undistinguishable from or equivalent to Er being equally distributed between Ti(1) and Ti(2) (0.017 in each octahedron). As with $Rb_{0.855}Ti_{0.955}Nb_{0.045}OPO_4$, Nb^{5+} tends to occupy Ti(1) positions to avoid electrostatic repulsion. This interpretation is reinforced by the fact that Er^{3+} cations, despite their lower electrical charge, do not show this tendency.

Initial Page **Table of Contents**